Spin-1/2 XY chain magnetoelectric: Effect of zigzag geometry

Ostap Baran,[1] Vadim Ohanyan,[2,3] and Taras Verkholyak[1]

[1]*Institute for Condensed Matter Physics, National Academy of Sciences of Ukraine, Svientsitskii Street 1, 79011 L'viv, Ukraine*

[2]*Department of Theoretical Physics, Yerevan State University, Alex Manoogian 1, 0025 Yerevan, Armenia*

[3]*Joint Laboratory of Theoretical Physics ICTP Affiliated Centre in Armenia, 2 A. Alikhanian Brothers Street, 0036 Yerevan, Armenia*

(Received 23 May 2018; revised manuscript received 19 June 2018; published 20 August 2018)

A spin-1/2 XY chain model of magnetoelectrics on a zigzag chain is considered rigorously. The magnetoelectric coupling is described within the Katsura-Nagaosa-Balatsky mechanism. In the zigzag geometry it leads to the staggered Dzyaloshinskii-Moriya interaction. Using nonuniform spin rotations, the model is reduced to a dimerized XY chain and solved exactly using the Jordan-Wigner transformation. We analyze the ground-state phase diagram of the model and the zero- and finite-temperature magnetoelectric effects and obtain the magnetization and polarization curves versus magnetic and electric fields, as well as the parameters of anisotropic dielectric and magnetoelectric response. It is also shown that the electric field may enhance the magnetocaloric effect in the model.

DOI: 10.1103/PhysRevB.98.064415

I. INTRODUCTION

Among multiferroics, materials simultaneously exhibiting more than one ferroic order [1–5], magnetoelectrics play a special role due to their broad and important technical applications [1]. The magnetoelectric effect (MEE) is, in general, the term for denoting the vast class of phenomena of intercoupling of magnetization and polarization in matter [1–3]. The most common manifestation of the MEE in solids is the magnetization dependence on the electric field and polarization dependence on the magnetic field. The magnetoelectric materials in general and the spin-related ferroelectricity are particularly important for possible application in various electronic and spintronic devices [4–8]. Moreover, there are more recent results evidencing the possibility to generate a field of a magnetic monopole by placing an electric charge on the surface of a linear magnetoelectric slab [9]. There exist several physical mechanisms coupling the local magnetic moments of the magnetic material with the local polarization of the unit cell. The one that will be considered in the present paper is based on the so-called spin current model, or inverse Dzyaloshinskii-Moriya (DM) model, and is referred to as the Katsura-Nagaosa-Balatsky (KNB) mechanism [10,11]. The KNB mechanism [10,11] links the dielectric polarization corresponding to the pair of spins at the adjacent lattice sites with the spin current across the bond given by the following expression:

$$\mathbf{P}_{ij} = \gamma \mathbf{e}_{ij} \times \mathbf{s}_i \times \mathbf{s}_j, \tag{1.1}$$

where $\mathbf{e}_{ij}$ is the unit vector pointing from site i to site j and γ is the coefficient that connects the electric polarization with the magnetic current operator.

Several exact results are known for the magnetoelectric models with the KNB mechanism [10,11]: the spin-1/2 XXZ chain [12], the spin-1/2 XY chain with three-spin interaction [13,14], and the generalized quantum compass model with magnetoelectric coupling [15]. The results of Refs. [12,13] were further confirmed in Refs. [16,17]. The link between DM terms and the quantum phase transitions of a generalized compass chain with staggered Dzyaloshinskii-Moriya interaction was also considered recently [18].

There are a number of real magnetic materials with a one-dimensional or quasi-one-dimensional magnetic lattice in which the MEE is realized according to the KNB mechanism [19–28]. For materials like $LiCu_2O_2$ [19–22], $LiCuVO_4$ [23–25], copper halides [26–28], and others, a more or less adequate model describing the MEE is believed to be the so-called multiferroic spin chain (MSC), the $S = 1/2$ quantum spin chain with competing ferromagnetic nearest-neighbor and antiferromagnetic next-nearest-neighbor interactions:

$$\mathcal{H} = J_1 \sum_{j=1}^{N} \mathbf{s}_j \cdot \mathbf{s}_{j+1} + J_2 \sum_{j=1}^{N} \mathbf{s}_j \cdot \mathbf{s}_{j+2} - \mathbf{E} \cdot \mathbf{P} - \mathbf{B} \cdot \mathbf{M}. \tag{1.2}$$

Here the electric (magnetic) field vector $\mathbf{E}$ ($\mathbf{B}$) is coupled to polarization (magnetization), given by

$$\mathbf{P} = \gamma \sum_{j=1}^{N} \left(\mathbf{s}_j \, s_{j+1}^x - s_j^x \, \mathbf{s}_{j+1} \right), \qquad \mathbf{M} = g\mu_B \sum_{j=1}^{N} \mathbf{s}_j, \tag{1.3}$$

respectively. Here g is the g factor of a magnetic ion, and μ_B is the Bohr magneton.

The chain is supposed to have a strictly linear form in the x direction. In addition to the MEE itself, the MSC recently received a considerable amount of attention in various other contexts, e.g., quantum information processing [29], quantum Otto cycles [30], pulse and quench dynamics [31], many-body localization [32], etc. It is worth mentioning that the physics of the MSC is very rich and complicated even without the electric field [33–38]. However, by virtue of its complexity the model (1.2) allows only numerical treatment. Nevertheless, the exact solutions of the simplified spin models demonstrating

the MEE due to the KNB mechanism are very important as they can shed light on the general universal properties of the magnetoelectrics and offer a unique opportunity to figure out their general features analytically [12–18]. In a previous work the integrable model of the $S = 1/2$ XXZ chain with DM interaction was considered as a model of the linear spin chain with the KNB mechanism [12]. MEE in this system has been shown to be trivial, which means the absence of polarization (magnetization) at zero external electric (magnetic) field. However, the magnetic (electric) field affects the polarization (magnetization) when the electric (magnetic) field is on. The next exactly solvable linear spin chain model with KNB mechanism, the XX chain with three-spin interactions [13,14], demonstrates nontrivial MEE; that is, only magnetic (electric) field can induce polarization (magnetization). This takes place due to three-spin terms, which mimic a microscopic interaction between local magnetic moment and local polarization.

In the present paper we continue our research on exactly solvable spin models with the KNB mechanism. However, as the form of the local polarization is essentially dependent on the geometry of the exchange interaction bonds between the spins, here we consider the effects of nonuniform local polarization throughout the chain. In the simplest case the local polarization for the bonds has a period of 2. Within the KNB mechanism this can be the case if one considers the chain to be folded to form a zigzag. Thus, formally, we deal with the XX model with alternating DM terms in the magnetic field. With the aid of the Jordan-Wigner transformation the system is mapped into the free spinless fermions. We studied in detail the zero- and finite-temperature magnetothermal and magnetoelectric properties of the model.

Although the model we study in the present work has no exact realization among the multiferroic materials known at the moment, the exact treatment and analytical results obtained in this paper can shed light on the general and universal features of the MEE in the case of the staggered local polarization as well as on the influence of the zigzag geometry of the bonds on the KNB mechanism. For instance, we obtained several universal results about the direction of the total polarization vector which can easily be generalized to the more realistic quantum spin chain models (see Appendixes A and B). Moreover, due to the ongoing progress in material science, the relevance of the model considered in the present paper will be possible to check using novel materials in the near future.

This paper is organized as follows: in the Sec. II we describe the KNB mechanism for the zigzag geometry; Sec. III presents the exact solution for the XY model of a magnetoelectric on a zigzag chain. In Sec. IV we describe its ground-state properties, including the zero-temperature MEE, and Sec. V is devoted to the finite-temperature properties of the model and MEE. Section VI concludes the paper.

II. KNB MECHANISM FOR SPIN CHAINS: THE INFLUENCE OF THE GEOMETRY

The form of the expression for the dielectric polarization in terms of the spin operators for the magnetoelectric material with KNB mechanism essentially depends on the geometry of the magnetic unit cell. For the linear chain in direction x ($\mathbf{e}_{ij} \equiv \mathbf{e}_x$) the corresponding expressions for the polarization vector components can be recovered from Eq. (1.1) and are quite simple [12–14]:

$$\begin{aligned} P^x_{j,j+1} &= 0, \\ P^y_{j,j+1} &= \gamma\left(s^y_j s^x_{j+1} - s^x_j s^y_{j+1}\right), \\ P^z_{j,j+1} &= \gamma\left(s^z_j s^x_{j+1} - s^x_j s^z_{j+1}\right). \end{aligned} \tag{2.1}$$

However, even small changes in the spatial arrangement of the spins can bring sufficient complication of the structure of local polarization. For instance, one can consider the spin chain lying in the xy plain but with the possibility of the arbitrary planar angle θ_j between the x axis and jth bond connecting the jth and $(j+1)$th sites. Then, the expression for the dielectric polarization corresponding to the jth bond should be modified according to the KNB formula, Eq. (1.1), and an altered direction of the bond should be given by the unit vector $\mathbf{e}_{j,j+1} = \cos\theta_j\ \mathbf{e}_x + \sin\theta_j\ \mathbf{e}_y$:

$$\mathbf{P}_{j,j+1} = \gamma(\cos\theta_j\ \mathbf{e}_x + \sin\theta_j\ \mathbf{e}_y) \times \mathbf{s}_j \times \mathbf{s}_{j+1}. \tag{2.2}$$

The corresponding components of the polarization are

$$\begin{aligned} P^x_{j,j+1} &= \gamma \sin\theta_j\left(s^x_j s^y_{j+1} - s^y_j s^x_{j+1}\right), \\ P^y_{j,j+1} &= -\gamma \cos\theta_j\left(s^x_j s^y_{j+1} - s^y_j s^x_{j+1}\right), \\ P^z_{j,j+1} &= \gamma \cos\theta_j\left(s^z_j s^x_{j+1} - s^x_j s^z_{j+1}\right) \\ &\quad + \sin\theta_j\left(s^z_j s^y_{j+1} - s^y_j s^z_{j+1}\right). \end{aligned} \tag{2.3}$$

Considering the constant and homogeneous electric field lying in the xy plain, $\mathbf{E} = (E_x, E_y, 0) = (E\cos\varphi_{\mathrm{E}}, E\sin\varphi_{\mathrm{E}}, 0)$, where φ_{E} is the angle between the x axis and the electric field vector, $E = \sqrt{E_x^2 + E_y^2}$, one can write down the energy contribution of the interaction between the dipole moment of the chain and electric field in the following form:

$$-\mathbf{E}\cdot\mathbf{P} = -E\gamma \sum_{j=1}^{N} \sin(\theta_j - \varphi_{\mathrm{E}})\left(s^x_j s^y_{j+1} - s^y_j s^x_{j+1}\right). \tag{2.4}$$

Let us now consider the same spin chain but bent to form a zigzag with fixed equal angles between the bonds (see Fig. 1). Therefore, the angle $\theta_j = (-1)^{j+1}\theta$ is staggered with respect to the x axis, and the polarization vectors between odd-even (bottom-top) and even-odd (top-bottom) pairs of spin are now

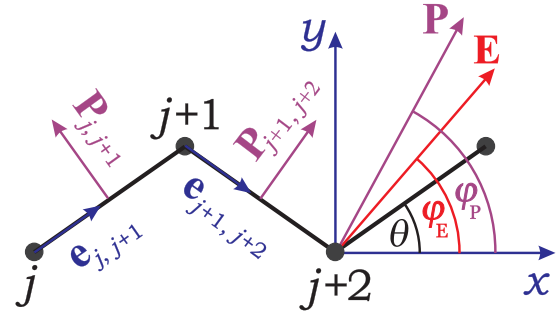

FIG. 1. The zigzag chain with indicated system axes, electric field vector $\mathbf{E}$, polarization $\mathbf{P}$, bond polarization $\mathbf{P}_{j,j+1}$, and unit vector $\mathbf{e}_{j,j+1}$ pointing from the jth site to the $(j+1)$th site. Here the z component of the bond polarization is equal zero because $\mathbf{E} = (E_x, E_y, 0)$.

different and are given by the following expressions:

$$\mathbf{P}_{j,j+1} = \gamma[\cos\theta \mathbf{e}_x - (-1)^j \sin\theta \mathbf{e}_y] \times \mathbf{s}_j \times \mathbf{s}_{j+1}. \quad (2.5)$$

Thus, Eq. (2.4) can be explicitly written as follows:

$$-\mathbf{E}\cdot\mathbf{P} = \gamma \sum_{j=1}^{N} [E_y \cos\theta + (-1)^j E_x \sin\theta]\left(s_j^x s_{j+1}^y - s_j^y s_{j+1}^x\right). \quad (2.6)$$

III. MODEL AND EXACT SOLUTION

We consider the quantum spin-1/2 XY model of N spins in the electric and magnetic field on the zigzag chain (see Fig. 1) described by the following Hamiltonian:

$$\mathcal{H} = \sum_{j=1}^{N} \left\{ J\left(s_j^x s_{j+1}^x + s_j^y s_{j+1}^y\right) + \gamma[E_y \cos\theta + (-1)^j E_x \sin\theta] \times \left(s_j^x s_{j+1}^y - s_j^y s_{j+1}^x\right)\right\} - h\sum_{j=1}^{N} s_j^z. \quad (3.1)$$

Here we introduce the renormalized magnetic field $h = g\mu_B B_z$. The first term in the Hamiltonian (3.1) refers to the superexchange coupling between neighboring spins, and the second [third] term corresponds to the energy of the model in the electric $\mathbf{E} = (E_x, E_y, 0)$ [magnetic $(0, 0, h)$] field. It can be noticed that the effect of the electric field discussed in the previous section is given by the staggered DM interaction terms. From Eqs. (2.6) and (3.1), we see that the coefficient γ appears only in the term of the electric field. Here we set $\gamma = 1$, bearing in mind that one has to use the specific value corresponding to each particular case of real materials. Thus, by comparing them to the experiment, our results for the polarization should be multiplied by γ, while the electric field needs to be divided by γ. In all further calculations we also set $J = 1$ and restrict ourselves to $0 < \theta < \pi/3$ since for larger values the distance between next-nearest neighbors become shorter than for the nearest neighbors. It should be mentioned that the model (3.1) resembles the two-sublattice XY chain with the DM interaction studied in Ref. [39], while the quantum compass model with the staggered DM interaction was considered recently in Ref. [18].

Here we face the case of isotropic XY interaction, where the Hamiltonian can be further simplified by the rotation transformation in the xy plain [40–44]:

$$\begin{aligned} \tilde{s}_j^x &= s_j^x \cos\phi_j + s_j^y \sin\phi_j, \\ \tilde{s}_j^y &= -s_j^x \sin\phi_j + s_j^y \cos\phi_j, \\ \tilde{s}_j^z &= s_j^z, \end{aligned} \quad (3.2)$$

where $\phi_{2j} = (j-1)(\phi^+ + \phi^-) + \phi^-$, $\phi_{2j+1} = j(\phi^+ + \phi^-)$, and $\tan\phi^\pm = E_\pm$. Hereinafter we use the notations $E_\pm = E_y\cos\theta \pm E_x \sin\theta \equiv E\sin(\varphi_E \pm \theta)$ and $E = \sqrt{E_x^2 + E_y^2}$. As a result we come to the dimerized XY chain considered in Ref. [45]:

$$\mathcal{H} = \sum_j \left\{[J_+ + (-1)^j J_-]\left(\tilde{s}_j^x \tilde{s}_{j+1}^x + \tilde{s}_j^y \tilde{s}_{j+1}^y\right) - h\tilde{s}_j^z\right\},$$
$$J_\pm = \frac{1}{2}\left(\sqrt{1+E_+^2} \pm \sqrt{1+E_-^2}\right). \quad (3.3)$$

It should be stressed that the described elimination of DM terms is possible only in the case of the nearest-neighbor interaction (see the discussions in Ref. [41]).

Using the Jordan-Wigner transformation [46], the model can be reduced to the noninteracting spinless fermion gas and then brought to the diagonal form by Fourier and unitary transformation (see details in Ref. [45]):

$$\mathcal{H} = \sum_{-\pi<k\leqslant\pi} \Lambda_k\left(a_k^+ a_k - \frac{1}{2}\right),$$
$$\Lambda_k = -h + \mathrm{sgn}(\cos k)\sqrt{J_+^2\cos^2 k + J_-^2 \sin^2 k}, \quad (3.4)$$

where a_k and a_k^+ are the Fermi annihilation and creation operators with quasimomentum $k = 2\pi l/N$ $(l = -N/2+1, \ldots, N/2)$ and Λ_k is the spectrum of the effective spinless fermion excitations of the dimerized model (3.3). The correspondence between the original spin model and its fermionic counterpart for linear XY magnetoelectrics can be found in Refs. [12,13]. Fermions create magnon excitations in the Hamiltonian (3.1), and the completely empty (filled) state corresponds to the fully polarized down- (up-) spin model.

We will take the thermodynamic limit in all further calculations. The free energy per site can be easily found as

$$f = -\frac{1}{\pi\beta}\int_0^\pi dk \ln\left[2\cosh\left(\frac{\beta\Lambda_k}{2}\right)\right], \quad (3.5)$$

where $\beta = \frac{1}{k_B T}$ is the inverse temperature T and k_B is the Boltzmann constant. All other thermodynamic quantities of the system can also be readily obtained by differentiating Eq. (3.5), i.e., the magnetization per site

$$m_z = \frac{1}{N}\sum_{j=1}^{N}\langle s_i^z\rangle = -\frac{1}{2\pi}\int_0^\pi dk \tanh\left(\frac{\beta\Lambda_k}{2}\right), \quad (3.6)$$

the x and y components of the electric polarization per site

$$\begin{aligned} p_\mu &= \frac{1}{N}\sum_{j=1}^{N}\langle P_{j,j+1}^\mu\rangle \\ &= \frac{1}{2\pi}\int_0^\pi dk\left(J_+\frac{\partial J_+}{\partial E_\mu}\cos^2 k + J_-\frac{\partial J_-}{\partial E_\mu}\sin^2 k\right) \\ &\quad\times \frac{\mathrm{sgn}(\cos k)\tanh\left(\frac{\beta\Lambda_k}{2}\right)}{\sqrt{J_+^2\cos^2 k + J_-^2\sin^2 k}}, \quad \mu = x, y, \end{aligned} \quad (3.7)$$

$$\frac{\partial J_\pm}{\partial E_x} = \frac{\sin\theta}{2}\left(\frac{E_+}{\sqrt{1+E_+^2}} \mp \frac{E_-}{\sqrt{1+E_-^2}}\right),$$
$$\frac{\partial J_\pm}{\partial E_y} = \frac{\cos\theta}{2}\left(\frac{E_+}{\sqrt{1+E_+^2}} \pm \frac{E_-}{\sqrt{1+E_-^2}}\right), \quad (3.8)$$

the entropy per site

$$S = \frac{k_B}{\pi}\int_0^\pi dk\left\{\ln\left[2\cosh\left(\frac{\beta\Lambda_k}{2}\right)\right] - \frac{\beta\Lambda_k}{2}\tanh\left(\frac{\beta\Lambda_k}{2}\right)\right\}, \quad (3.9)$$

and the specific heat per site

$$c = \frac{k_B \beta^2}{4\pi} \int_0^\pi dk \frac{\Lambda_k^2}{\cosh^2\left(\frac{\beta\Lambda_k}{2}\right)}. \tag{3.10}$$

The important physical quantity to characterize the MEE is the magnetoelectric susceptibility (magnetoelectric tensor), given by the following expression:

$$\alpha_{\mu\nu} = \left(\frac{\partial m_\mu}{\partial E_\nu}\right)_{T,\mathbf{B}} = \left(\frac{\partial P_\nu}{\partial h_\mu}\right)_{T,\mathbf{E}}. \tag{3.11}$$

In our case we have two components $\alpha_{z\mu}$ ($\mu = x, y$) of the magnetoelectric tensor:

$$\alpha_{z\mu} = -\frac{\beta}{4\pi} \int_0^\pi dk \frac{\mathrm{sgn}(\cos k)\left[J_+ \frac{\partial J_+}{\partial E_\mu} \cos^2 k + J_- \frac{\partial J_-}{\partial E_\mu} \sin^2 k\right]}{\cosh^2\left(\frac{\beta\Lambda_k}{2}\right)\sqrt{J_+^2 \cos^2 k + J_-^2 \sin^2 k}}. \tag{3.12}$$

Looking at the transformed Hamiltonian (3.3), one can notice some symmetries in the model. If the electric field is directed along only the y axis, the system evidently does not feel any zigzag deformation and behaves identically to the quantum XY model on a simple linear chain [12,13]. Interestingly, the direction of the field along the x axis, which corresponds to the staggered DM term, recovers the same limit of the linear chain. It is easy to check that in the former case $E_x \neq 0$, $E_y = 0$, the Hamiltonian (3.1) is explicitly dimerized, but the rotation (3.2) reduces it to the uniform form. Additionally, in the general case ($E_x \neq 0$, $E_y \neq 0$), if we choose $\phi_{2j-1} = \phi_{2j} = 2j\phi^-$ in the rotation transformation (3.2), we get the following relation between the transformed and initial Hamiltonians $\tilde{\mathcal{H}}(E_x \sin\theta, E_y \cos\theta) = \mathcal{H}(E_y \cos\theta, E_x \sin\theta)$. Thus, some thermodynamic functions (e.g., f, m_z, and c) are invariant under simultaneous exchanges $\theta \to \pi/2 - \theta$ and $E_x \leftrightarrow E_y$, while some electric characteristics are transformed according to simple relations (e.g., $p_x \leftrightarrow p_y$). It is also clear that the replacement $E_\mu \to -E_\mu$ changes only some electric characteristics (e.g., $p_\mu \to -p_\mu$). Therefore, without loss of generality we hereinafter restrict our investigation to the intervals $0 \leqslant \theta \leqslant \pi/4$ and $0 \leqslant \varphi_E \leqslant \pi/2$.

IV. GROUND-STATE PROPERTIES

The application of the electric field in the xy plane may transform the model into the effectively dimerized XY chain (3.3). As we show below it leads to the appearance of a new nonmagnetic gapped phase and a new topology of the ground-state phase diagram. For the sake of clarity, we choose $h \geqslant 0$. From the analysis of the excitation spectrum Λ_k (3.4), we deduce that the model is in the gapless spin-liquid phase if $|J_-| < h < J_+$ since the excitation spectrum Λ_k becomes zero at Fermi points $\pm k_0$, given by the expression

$$k_0 = \arcsin \frac{\sqrt{1 - (h/J_+)^2}}{\kappa}, \tag{4.1}$$

where $\kappa = \sqrt{1 - (J_-/J_+)^2}$. In the case $h < |J_-|$ we have a gapped zero-plateau phase, while for $h > J_+$ all spins are directed along the magnetic field. The ground-state phase diagrams as functions of electric and magnetic fields are shown in Figs. 2 and 3. One can see that the electric field destroys the saturated phase and drives the system to the spin-liquid gapless phase. Finally, for rather strong fields in the xy plain we obtained a completely demagnetized phase $m_z = 0$. It should be noted that negative values E_x and E_y are presented in Fig. 2 for the sake of clarity.

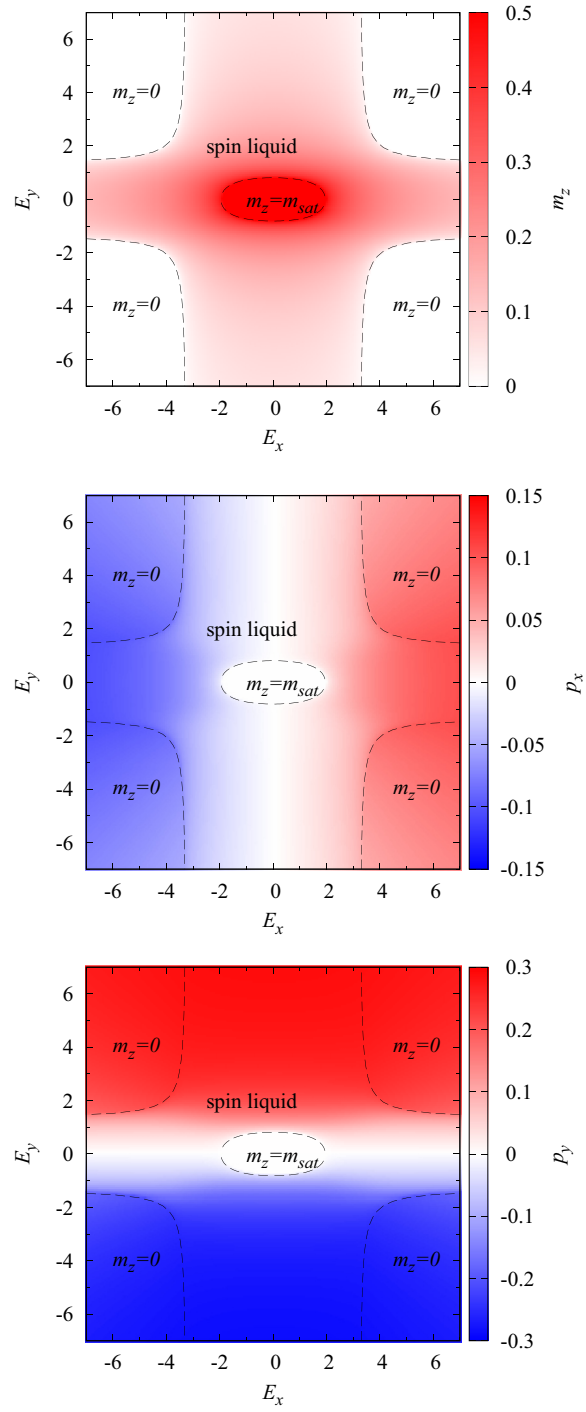

FIG. 2. Density plots for the magnetization (top panel) and polarizations p_x and p_y (middle and bottom panels) at $T = 0$ for $\theta = \pi/8$, $h = 1.25$. Dashed lines indicate the boundaries between different ground-state phases.

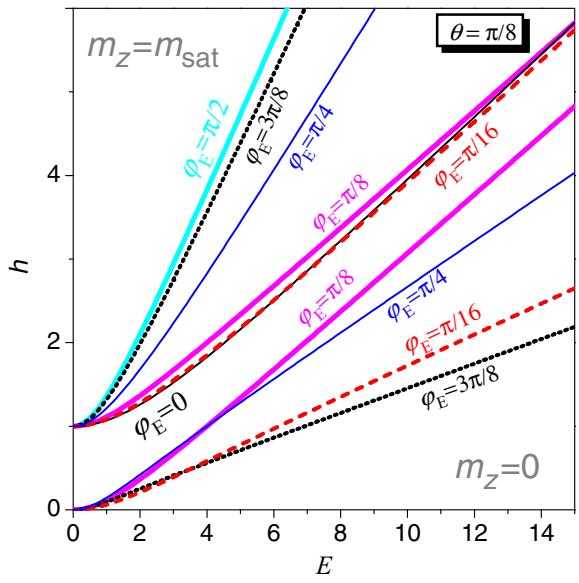

FIG. 3. The ground-state phase diagram for $\theta = \pi/8$ in different directions of the electric field $\varphi_E = 0, \pi/16, \pi/8, \pi/4, 3\pi/8, \pi/2$.

The ground-state energy corresponding to the $T \to 0$ limit is expressed as

$$e_0 = \begin{cases} -\frac{J_+}{\pi}\mathbf{E}(\kappa) & \text{if } h \leqslant |J_-|, \\ -\left(\frac{1}{2}-\frac{k_0}{\pi}\right)h-\frac{J_+}{\pi}\mathbf{E}(k_0|\kappa) & \text{if } |J_-|\leqslant h\leqslant J_+, \\ -\frac{h}{2} & \text{if } h \geqslant J_+, \end{cases} \quad (4.2)$$

where k_0 is the Fermi point given in Eq. (4.1), $\mathbf{E}(k_0|\kappa) = \int_0^{k_0} dk\sqrt{1-\kappa^2\sin^2 k}$ is the incomplete elliptic integral of the second kind of modulus κ, and $\mathbf{E}(\kappa) = \mathbf{E}(\pi/2|\kappa)$.

The ground-state magnetization can be obtained as

$$m_z = \begin{cases} 0 & \text{if } h \leqslant |J_-|, \\ \frac{1}{2}-\frac{k_0}{\pi} & \text{if } |J_-|\leqslant h\leqslant J_+, \\ \frac{1}{2} & \text{if } h \geqslant J_+. \end{cases} \quad (4.3)$$

The expressions for the electric polarization $p_\mu = -\frac{\partial e_0}{\partial E_\mu}$ ($\mu = x, y$) can be derived by a straightforward calculation. In the saturated phase $h > J_+$ it equals zero. In the spin-liquid state ($|J_-| < h < J_+$) it is given by the following expression:

$$p_\mu = \frac{1}{\pi}\left\{\frac{\partial J_+}{\partial E_\mu}\mathbf{E}(k_0|\kappa)+\frac{J_+}{2\kappa^2}[\mathbf{E}(k_0|\kappa)-\mathbf{F}(k_0|\kappa)]\frac{\partial\kappa^2}{\partial E_\mu}\right\},$$
$$\frac{\partial\kappa^2}{\partial E_\mu} = -\frac{2J_-}{J_+^2}\left(\frac{\partial J_-}{\partial E_\mu}-\frac{J_-}{J_+}\frac{\partial J_+}{\partial E_\mu}\right), \quad (4.4)$$

where $\mathbf{F}(k_0|\kappa) = \int_0^{k_0}\frac{dk}{\sqrt{1-\kappa^2\sin^2 k}}$ is the incomplete elliptic integral of the first kind and $\frac{\partial J_\pm}{\partial E_\mu}$ are given in Eq. (3.8). For the nonmagnetic phase ($h < |J_-|$) we get

$$p_\mu = \frac{1}{\pi}\left\{\frac{\partial J_+}{\partial E_\mu}\mathbf{E}(\kappa)+\frac{J_+}{2\kappa^2}[\mathbf{E}(\kappa)-\mathbf{K}(\kappa)]\frac{\partial\kappa^2}{\partial E_\mu}\right\}, \quad (4.5)$$

where $\mathbf{K}(\kappa) = \mathbf{F}(\pi/2|\kappa)$.

The polarization is a nonanalytic function in zero magnetic and electric fields. To show that, we can use an asymptotic expansion for the complete elliptic integral of the first kind for $\kappa \approx 1$:

$$\mathbf{K}(\kappa) = \tfrac{1}{2}\ln(1-\kappa^2) + O(1). \quad (4.6)$$

Thus, the low-field expansion of the electric polarization reveals the logarithmic nonanalytical behavior:

$$p_x \approx \frac{1}{\pi}\left\{E_x\sin^2\theta-\frac{1}{4}E_xE_y^2\sin^2(2\theta)\ln|E_xE_y\sin(2\theta)|\right\},$$
$$p_y \approx \frac{1}{\pi}\left\{E_y\cos^2\theta-\frac{1}{4}E_x^2E_y\sin^2(2\theta)\ln|E_xE_y\sin(2\theta)|\right\}. \quad (4.7)$$

In particular, as seen from these equations, there is a singularity in the fourth derivative of the ground-state energy $\partial^4 e_0/(\partial E_x^2\partial E_y^2)$ [see Eq. (4.7)].

The electric field dependence of the magnetization and polarization at $T = 0$ is shown in Figs. 4 and 5. One can notice the demagnetizing effect of the electric field when increasing field at first destroys the completely ordered phase and leads to the gapless spin-liquid phase. At the end, the gapped phase with zero magnetization emerges. Predictably, the electric polarization has the opposite behavior. It starts from zero value in small electric fields passing through the spin-liquid phase to the nonmagnetic gapped phase. Interestingly, the electric polarization does not achieve the saturation value for a finite electric field. One can also note that when the magnetic field $h < J_+$ the polarization immediately emerges with the electric field with the linear law.

Figure 6 demonstrates the explicit dependence of the magnetization and polarization characteristics on the magnetic field. We see that the electric field applied in the xy plain induces the gap in the excitation spectrum and the zero plateau in the magnetization curve. In the zero-plateau phase the polarization does not depend on the magnetic field according to Eq. (4.5).

A. The polarization angle

It is useful to follow the behavior of the polarization angle φ_P (between the x axis and the vector of electric polarization) in applied electric and magnetic fields (Figs. 4–6). It is worth mentioning that if $\varphi_E \in (0, \pi/2)$ and $\theta \in (0, \pi/4)$ and, additionally, $\varphi_E > \theta$, the polarization angle is larger than θ at any magnitude of the electric and magnetic fields, while φ_P can be larger or smaller than φ_E depending on the values of the parameters θ, h, and E. In the general case the angle of $\mathbf{P}$ can be greater or less than both θ and φ_E. Obviously, $\varphi_P \in [0, \pi/2]$ at $\varphi_E \in [0, \pi/2]$. It is also interesting that in the case $0 < \varphi_E < \theta$ the polarization angle φ_P is an increasing function of the strength of the electric field at small enough and sufficiently large values of h, while at intermediate values of magnetic field $\varphi_P(E)$ is a nonmonotonous function with one minimum. In the case $\theta < \varphi_E < \pi/2$ the behavior of the polarization angle is the reverse: $\varphi_P(E)$ is a decreasing or nonmonotonous function with one maximum. The magnetic field dependence of φ_P is affected by the relation between φ_E and θ. In the spin-liquid phase $\varphi_P(h)$ is a decreasing (increasing) function at $0 < \varphi_E < \theta$ ($\theta < \varphi_E < \pi/2$).

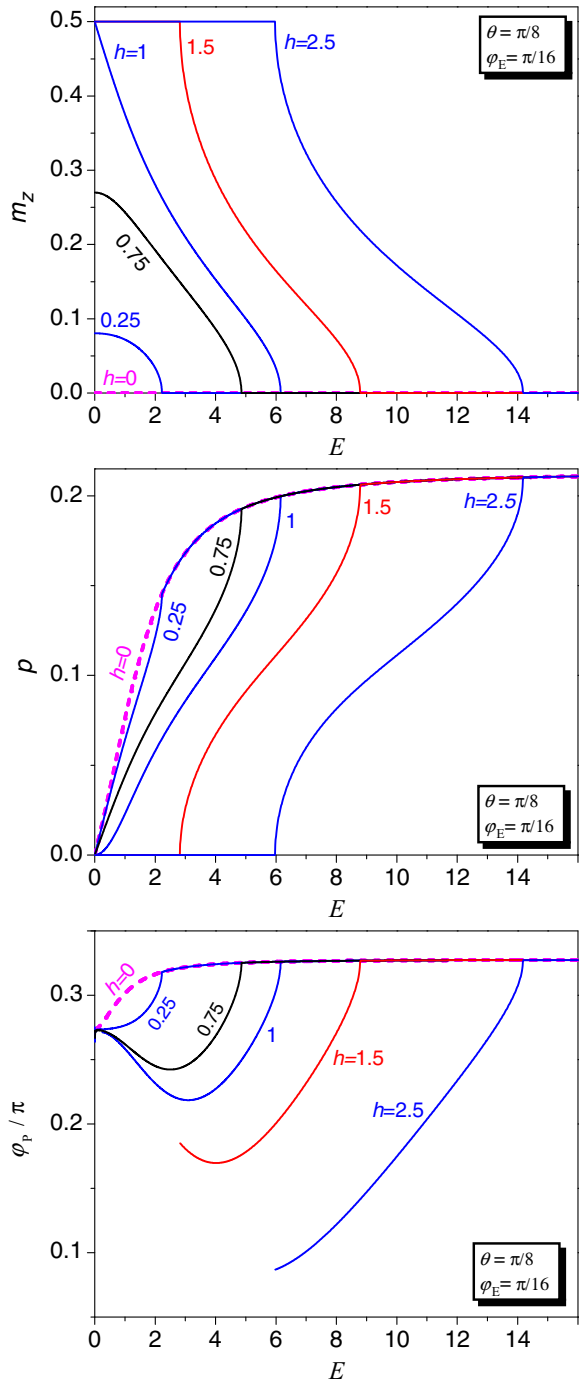

FIG. 4. The magnetization (top panel), the absolute value (middle panel), and the angle (bottom panel) of the electric polarization vs electric field for $\theta = \pi/8$, $\varphi_E = \pi/16$, and different magnetic fields $h = 0, 0.25, 0.75, 1, 1.5, 2.5$.

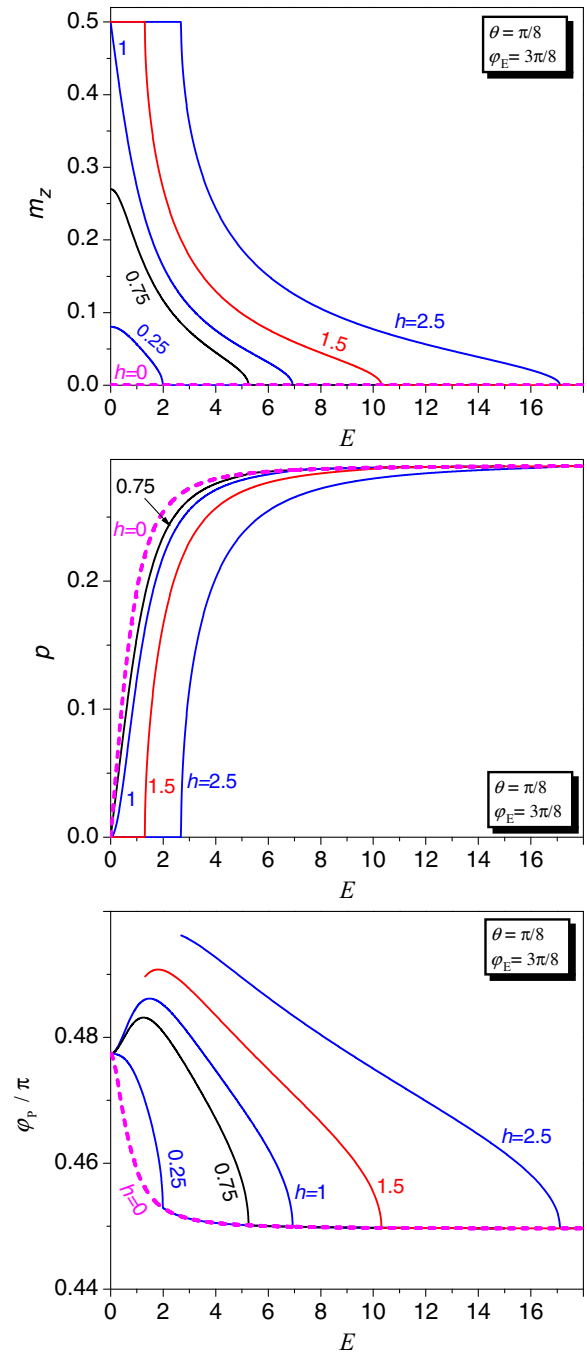

FIG. 5. The magnetization (top panel), the absolute value (middle panel), and the angle (bottom panel) of the electric polarization vs electric field for $\theta = \pi/8$, $\varphi_E = 3\pi/8$, and different magnetic fields $h = 0, 0.25, 0.75, 1, 1.5, 2.5$.

If the electric field is directed along some of the bonds (e.g., $\varphi_E = \theta$), φ_P does not depend on the strength of the electric and magnetic fields. It can be shown explicitly calculating $\tan\varphi_P = p_y/p_x$. Using Eqs. (4.4) and (4.5), we can easily get the expression

$$\tan\varphi_P = \frac{1+\xi(E,\theta)}{1-\xi(E,\theta)}\cot\theta, \tag{4.8}$$

where

$$\xi(E,\theta) = \frac{E_-(1+E_+^2)\left[\mathbf{E}(k_0|\kappa) - \frac{J_-}{J_+}\mathbf{F}(k_0|\kappa)\right]}{E_+(1+E_-^2)\left[\mathbf{E}(k_0|\kappa) + \frac{J_-}{J_+}\mathbf{F}(k_0|\kappa)\right]}$$

for the spin-liquid state ($|J_-| < h < J_+$), while one should set $k_0 = \pi/2$ in the case of the nonmagnetic phase ($h < |J_-|$). At $\varphi_E = \theta$ one has $E_- = 0$, and Eq. (4.8) leads to the relation

$$\tan\varphi_P = \cot\theta \quad \text{if } \varphi_E = \theta. \tag{4.9}$$

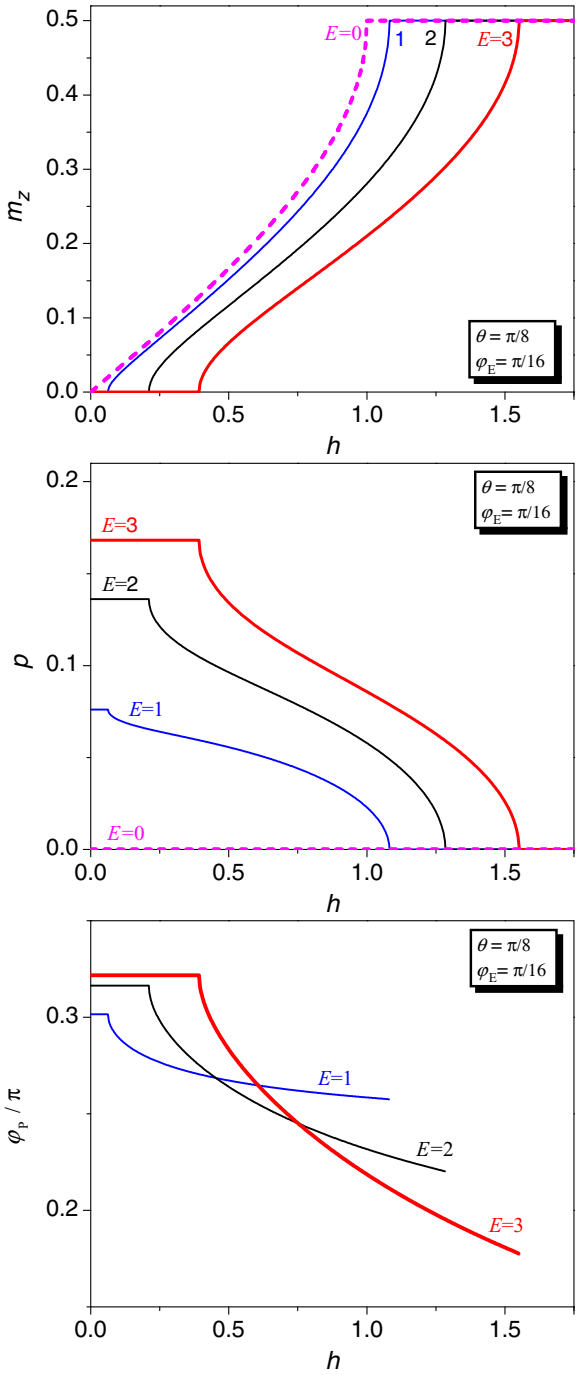

FIG. 6. The magnetization (top panel) the absolute value (middle panel), and the angle (bottom panel) of the electric polarization vs magnetic field for $\theta = \pi/8$, $\varphi_{\rm E} = \pi/16$, and different electric fields $E = 0, 1, 2, 3$.

As a consequence, the polarization is orthogonal to the direction of nonparallel bonds:

$$\varphi_{\rm P} = \frac{\pi}{2} - \theta \quad \text{if } \varphi_{\rm E} = \theta. \tag{4.10}$$

This simple result can be readily understood from the basic description of the model (3.1). If the electric field and one type of bond are collinear, the electric polarization cannot be created there due to the specific feature of the KNB mechanism (1.1). At the same time it induces a nonzero polarization perpendicular to the direction of other bonds. Such arguments are quite general and are valid for nonzero temperatures and the more general XXZ model as well but cannot be applied to a model with the next-nearest neighbor interaction (see Appendix A).

There are several examples where the dependence of $\varphi_{\rm P}$ on $\varphi_{\rm E}$ is universal. In the case of strong electric fields $E \to \infty$, the details of the exchange interactions become irrelevant. The system is governed exclusively by the electric field. Taking the limit $E \to \infty$ for fixed $\varphi_{\rm E}$ in Eq.(4.5), we get

$$\tan\varphi_{\rm P} = -\frac{\tan\varphi_{\rm E}}{\tan^2\theta}\,\frac{\mathbf{E}(\kappa') - \mathbf{K}(\kappa')}{\mathbf{E}(\kappa') - \left(\frac{\tan\varphi_{\rm E}}{\tan\theta}\right)^2\mathbf{K}(\kappa')},$$

$$\kappa' = \lim_{E\to\infty}\kappa = \sqrt{1 - \left(\frac{\tan\varphi_{\rm E}}{\tan\theta}\right)^2}$$

$$\text{if } \varphi_{\rm E} < \theta;$$

$$\tan\varphi_{\rm P} = -\frac{\tan\varphi_{\rm E}}{\tan^2\theta}\,\frac{\mathbf{E}(\kappa'') - \left(\frac{\tan\theta}{\tan\varphi_{\rm E}}\right)^2\mathbf{K}(\kappa'')}{\mathbf{E}(\kappa'') - \mathbf{K}(\kappa'')},$$

$$\kappa'' = \lim_{E\to\infty}\kappa = \sqrt{1 - \left(\frac{\tan\theta}{\tan\varphi_{\rm E}}\right)^2}$$

$$\text{if } \varphi_{\rm E} > \theta. \tag{4.11}$$

This result shows that such a dependence characterizes only the geometry of the lattice but not the spin model itself. It is also useful to estimate the dependence when the electric field is directed close to the x or y axis. Thus, at $E \to \infty$ and $\theta \neq 0$ we have

$$\tan\varphi_{\rm P} = -\frac{\tan\varphi_{\rm E}}{\tan^2\theta}\ln\left|\frac{\tan\varphi_{\rm E}}{\tan\theta}\right| \quad \text{if } \varphi_{\rm E} \to 0,$$

$$\cot\varphi_{\rm P} = -\frac{\tan\varphi_{\rm E}}{\cot^2\theta}\ln\left|\frac{\tan\varphi_{\rm E}}{\cot\theta}\right| \quad \text{if } \varphi_{\rm E} \to \frac{\pi}{2}. \tag{4.12}$$

In the case of low fields $E \to 0$, we can keep the first terms in Eq. (4.7) to get

$$\tan\varphi_{\rm P} = \frac{\tan\varphi_{\rm E}}{\tan^2\theta}. \tag{4.13}$$

In Appendix B we show that this result is also valid for XXZ magnetoelectrics on a zigzag chain.

The results for the polarization angle can be seen in Fig. 7. Both Eqs. (4.11) and (4.13) recover the limit $\varphi_{\rm E} = \theta$, and as one can see, the corresponding curves cross at this point. For small enough values of θ the polarization angle is larger than $\varphi_{\rm E}$ both at $E \to 0$ and at $E \to \infty$. For $\theta \to \pi/4$ one has $\varphi_{\rm P} \approx \varphi_{\rm E}$ at $E \to 0$, while at $E \to \infty$ the polarization angle is larger (smaller) than $\varphi_{\rm E}$ if $\varphi_{\rm E} < \pi/4$ ($\varphi_{\rm E} > \pi/4$).

B. Susceptibilities

There are three kinds of susceptibilities in our system, electric, magnetic, and mixed, i.e., magnetoelectric.

The expressions for the electric susceptibilities per site $\chi_{\mu\nu} = \frac{\partial p_\mu}{\partial E_\nu}$ ($\mu = x, y$) can be found with a straightforward calculation. In the saturated phase they equal zero. In the spin-liquid state [where k_0 is given in Eq. (4.1)] and in the

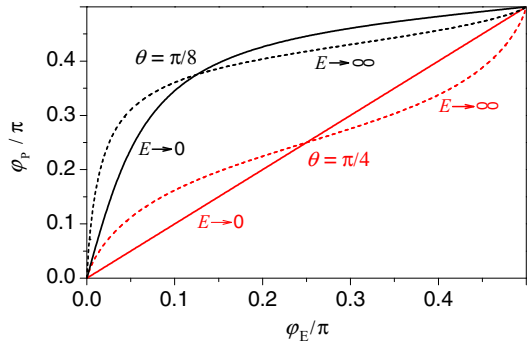

FIG. 7. The polarization angle $\varphi_{\rm P}$ as a function of the electric field angle $\varphi_{\rm E}$ for infinitesimally small (solid line) and infinite (dashed line) electric fields at $\theta = \pi/8, \pi/4$.

nonmagnetic phase (where $k_0 = \pi/2$) we get

$$\chi_{\mu\nu} = \frac{1}{\pi}\left\{\frac{\partial^2 J_+}{\partial E_\mu \partial E_\nu}\mathbf{E}(k_0|\kappa) + \left[\frac{h}{J_+}\frac{\partial J_+}{\partial E_\mu} + \frac{h^2 - J_+^2}{2h\kappa^2}\frac{\partial \kappa^2}{\partial E_\mu}\right]\frac{\partial k_0}{\partial E_\nu} + \frac{J_+}{4\kappa^2(1-\kappa^2)}\left[\frac{J_+}{h}\sin k_0 \cos k_0 - \mathbf{F}(k_0|\kappa)\right]\frac{\partial \kappa^2}{\partial E_\mu}\frac{\partial \kappa^2}{\partial E_\nu} + \frac{1}{2\kappa^2}[\mathbf{E}(k_0|\kappa) - \mathbf{F}(k_0|\kappa)]\left[\frac{\partial J_+}{\partial E_\mu}\frac{\partial \kappa^2}{\partial E_\nu} + \frac{\partial J_+}{\partial E_\nu}\frac{\partial \kappa^2}{\partial E_\mu} + J_+\frac{\partial^2 \kappa^2}{\partial E_\mu \partial E_\nu} - J_+\frac{2-\kappa^2}{2\kappa^2(1-\kappa^2)}\frac{\partial \kappa^2}{\partial E_\mu}\frac{\partial \kappa^2}{\partial E_\nu}\right]\right\}. \quad (4.14)$$

Here $\frac{\partial J_\pm}{\partial E_\mu}$, $\frac{\partial \kappa^2}{\partial E_\mu}$ are given in Eqs. (3.8) and (4.4), and $\frac{\partial k_0}{\partial E_\mu} = 0$ in the nonmagnetic phase, while

$$\frac{\partial k_0}{\partial E_\mu} = \frac{J_+(h^2 - J_-^2)\frac{\partial J_+}{\partial E_\mu} + J_-(J_+^2 - h^2)\frac{\partial J_-}{\partial E_\mu}}{(J_+^2 - J_-^2)\sqrt{(J_+^2 - h^2)(h^2 - J_-^2)}} \quad (4.15)$$

in the spin-liquid state. The derivatives used in Eqs. (4.14) and(4.15) are given by the following expressions:

$$\frac{\partial^2 \kappa^2}{\partial E_\mu \partial E_\nu} = \frac{2J_-}{J_+^2}\left[\frac{J_-}{J_+}\frac{\partial^2 J_+}{\partial E_\mu \partial E_\nu} - \frac{\partial^2 J_-}{\partial E_\mu \partial E_\nu}\right] + \frac{4J_-}{J_+^3}\left[\frac{\partial J_+}{\partial E_\mu}\frac{\partial J_-}{\partial E_\nu} + \frac{\partial J_-}{\partial E_\mu}\frac{\partial J_+}{\partial E_\nu}\right] - \frac{2}{J_+^2}\left[\frac{\partial J_-}{\partial E_\mu}\frac{\partial J_-}{\partial E_\nu} + \frac{3J_-^2}{J_+^2}\frac{\partial J_+}{\partial E_\mu}\frac{\partial J_+}{\partial E_\nu}\right],$$

$$\frac{\partial^2 J_\pm}{\partial E_x^2} = B_\pm \sin^2\theta, \quad \frac{\partial^2 J_\pm}{\partial E_y^2} = B_\pm \cos^2\theta,$$

$$\frac{\partial^2 J_\pm}{\partial E_x \partial E_y} = B_\pm \sin\theta\cos\theta,$$

$$B_\pm = \frac{1}{2(1+E_+^2)^{3/2}} \pm \frac{1}{2(1+E_-^2)^{3/2}}. \quad (4.16)$$

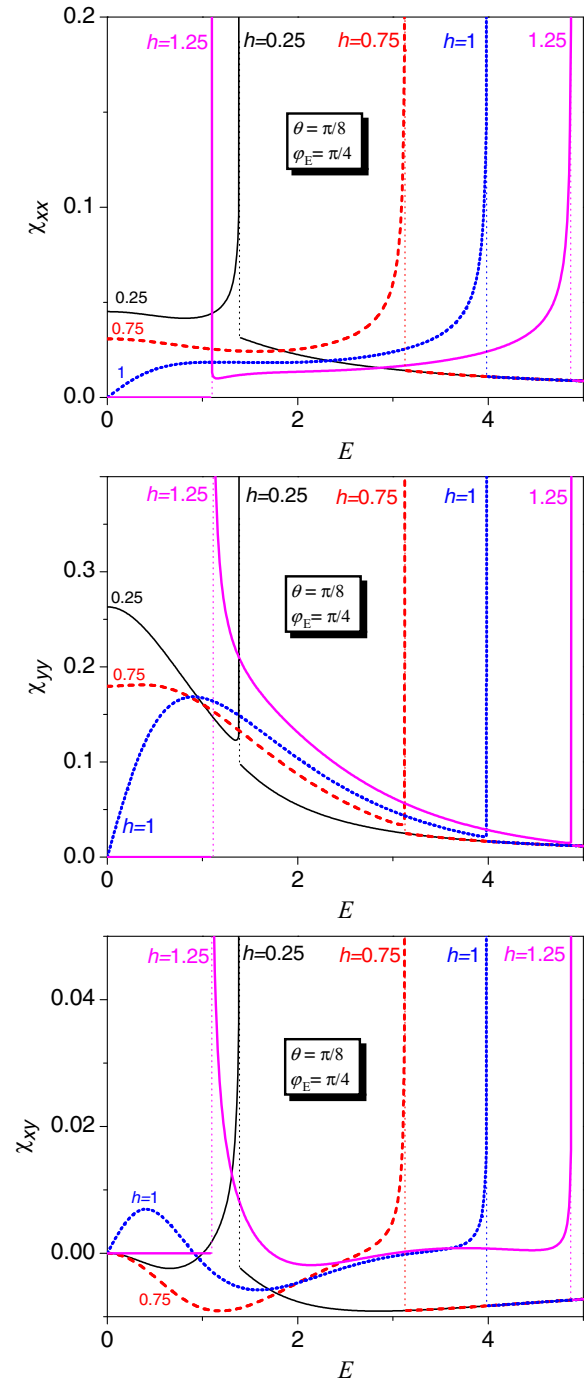

FIG. 8. The electric susceptibilities χ_{xx}, χ_{yy}, and χ_{xy} at $T = 0$ as a function of the electric field for $\theta = \pi/8$, $\varphi_{\rm E} = \pi/4$, and different values of h.

It is obvious that electric susceptibilities exhibit van Hove singularities along the boundaries of the spin-liquid phase. The most representative plots for the case when θ is substantially smaller than $\varphi_{\rm E}$ (e.g., $\theta = \pi/8$, $\varphi_{\rm E} = \pi/4$) for the electric and magnetic field dependence of the components of the zero-temperature electric susceptibility of the system, both diagonal (χ_{xx} and χ_{yy}) and off-diagonal (χ_{xy}), are presented in Figs. 8 and 9, respectively. The singular peaks at the points of the quantum phase transitions are well pronounced here.

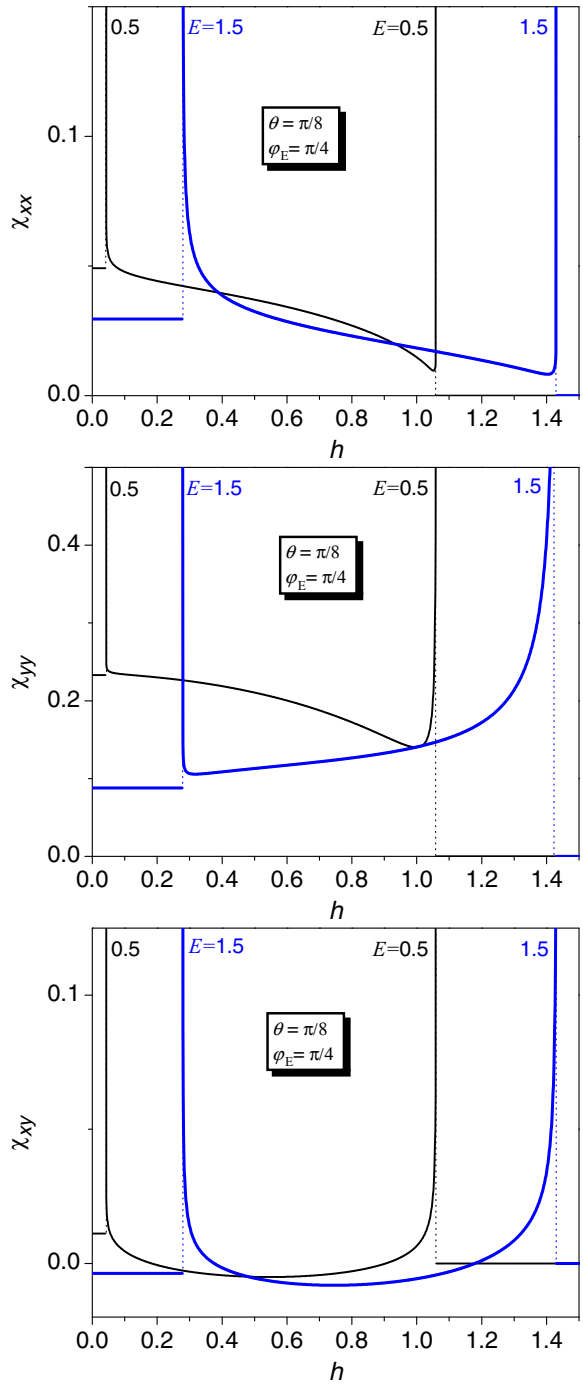

FIG. 9. The electric susceptibilities χ_{xx}, χ_{yy}, and χ_{xy} at $T = 0$ as a function of the magnetic field for $\theta = \pi/8$, $\varphi_{\mathrm{E}} = \pi/4$, and different values of E.

The magnetic susceptibility per site $\chi_{zz} = \frac{\partial m_z}{\partial h}$ in the spin-liquid state is quite simple:

$$\chi_{zz} = \frac{1}{\pi} \frac{h}{\sqrt{(J_+^2 - h^2)(h^2 - J_-^2)}}, \tag{4.17}$$

while in the saturated and nonmagnetic phases it equals zero. The corresponding plots of the $T = 0$ magnetic susceptibility exhibiting the peaks pointing to the critical values of the electric and magnetic fields can be found in Fig. 10 for $\theta = \pi/8$ and $\varphi_{\mathrm{E}} = \pi/4$.

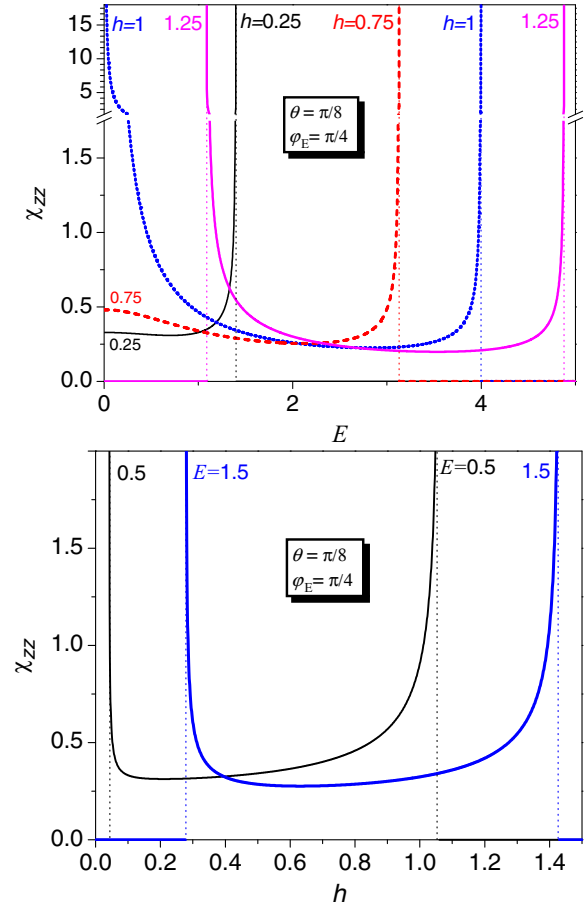

FIG. 10. The magnetic susceptibility χ_{zz} at $T = 0$ as a function of the electric field (top panel) and the magnetic field (bottom panel) for $\theta = \pi/8$, $\varphi_{\mathrm{E}} = \pi/4$.

The magnetoelectric tensor components in the ground state can be obtained from the zero-temperature limit of Eq. (3.12), or by directly taking the derivatives of Eq. (4.3),

$$\alpha_{z\mu} = \begin{cases} 0 & \text{if } h < |J_-|, \\ -\frac{1}{\pi} \frac{\partial k_0}{\partial E_\mu} & \text{if } |J_-| \leqslant h \leqslant J_+, \\ 0 & \text{if } h > J_+, \end{cases} \tag{4.18}$$

where $\mu = x, y$ and the explicit form of the corresponding derivative of the Fermi momenta is given in Eq. (4.15). It should be noted that the magnetoelectric tensor components and the magnetic susceptibility equal zero outside the spin-liquid phase, while electric susceptibilities equal zero in only the saturated phase.

The corresponding plots of the zero-temperature magnetoelectric tensor's nonzero components' dependence on electric and magnetic fields are presented in Fig. 11 for $\theta = \pi/8$ and $\varphi_{\mathrm{E}} = \pi/4$. It is seen that the magnetoelectric tensor exhibits a square-root van Hove singularities along the boundaries of the spin-liquid phase. The same feature can be found in the behavior of the magnetic and electric susceptibilities (see Figs. 8–10). It is interesting to observe that the magnetoelectric tensor is always zero for $E = 0$ except in the case when the

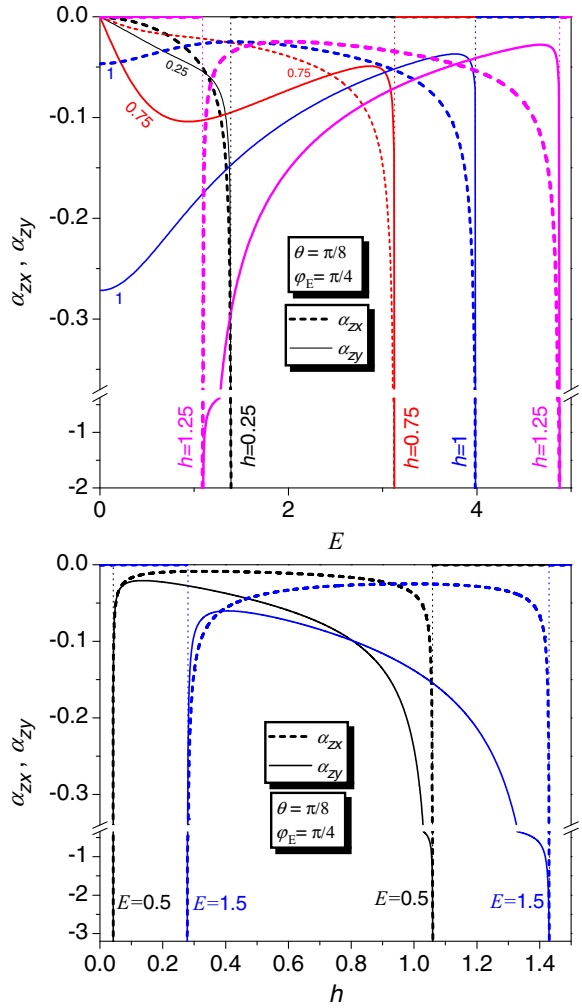

FIG. 11. The magnetoelectric tensor at $T = 0$ as a function of the electric field (top panel) and the magnetic field (bottom panel) for $\theta = \pi/8$, $\varphi_E = \pi/4$.

magnetic field is at its critical value. This result follows directly from Eq. (4.15) in the limit $E \to 0$ at $h = J = 1$. It should also be noted that in the case $h < 1$ the zy component of the magnetoelectric tensor at sufficiently small values of h is a decreasing function of E, whereas at sufficiently large values of magnetic field it is a nonmonotonic function (see Fig. 11 at $h = 0.25$ and $h = 0.75$).

In the case when θ is substantially larger than φ_E the results for ground-state susceptibilities are somewhat different. For example (see Figs. 8 and 11), at $\theta < \varphi_E$ the curves of $\chi_{xx}(E)$ and $\alpha_{zx}(E)$ demonstrate sharper behavior near the saturated phase than near the nonmagnetic one in the spin-liquid phase, while the curves of $\chi_{yy}(E)$ and $\alpha_{zy}(E)$ have a sharper course near the nonmagnetic phase than near the saturated one. At $\theta > \varphi_E$ we have the opposite situation.

V. THERMODYNAMICS

In this section we discuss the features of the temperature effect in the zigzag magnetoelectric. Let us start with the temperature-dependent specific heat, which can show different behaviors in various phases (see Fig. 12).

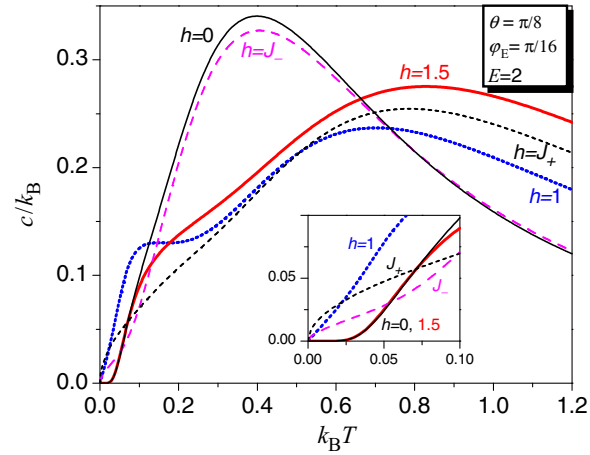

FIG. 12. Specific heat as a function of temperature for $\theta = \pi/8$, $\varphi_E = \pi/16$, $E = 2$, $h = 0$, J_-, 1, J_+, 1.5.

In the gapped zero-magnetization and saturated phases we get the exponential asymptote in the low-temperature specific heat, while the spin-liquid phase is characterized by a power-law dependence on temperature [47]. In our case we get the linear dependence on the temperature for $|J_-| < h < J_+$, which can clearly be seen in the inset of Fig. 12. The most

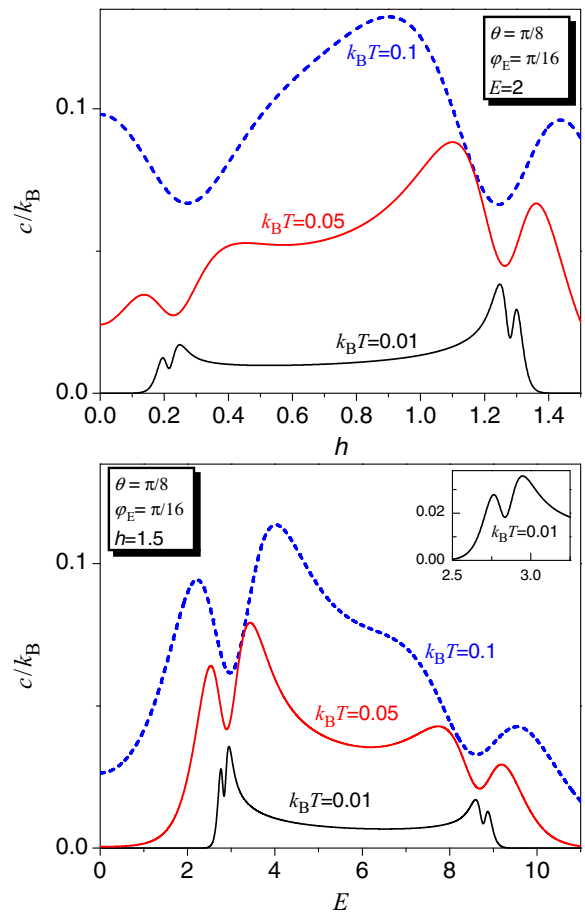

FIG. 13. Specific heat as a function of the magnetic field (top panel) for $E = 2$ and of the electric field (bottom panel) for $h = 1.5$ and $\theta = \pi/8$, $\varphi_E = \pi/16$, $T = 0.01, 0.05, 0.1$.

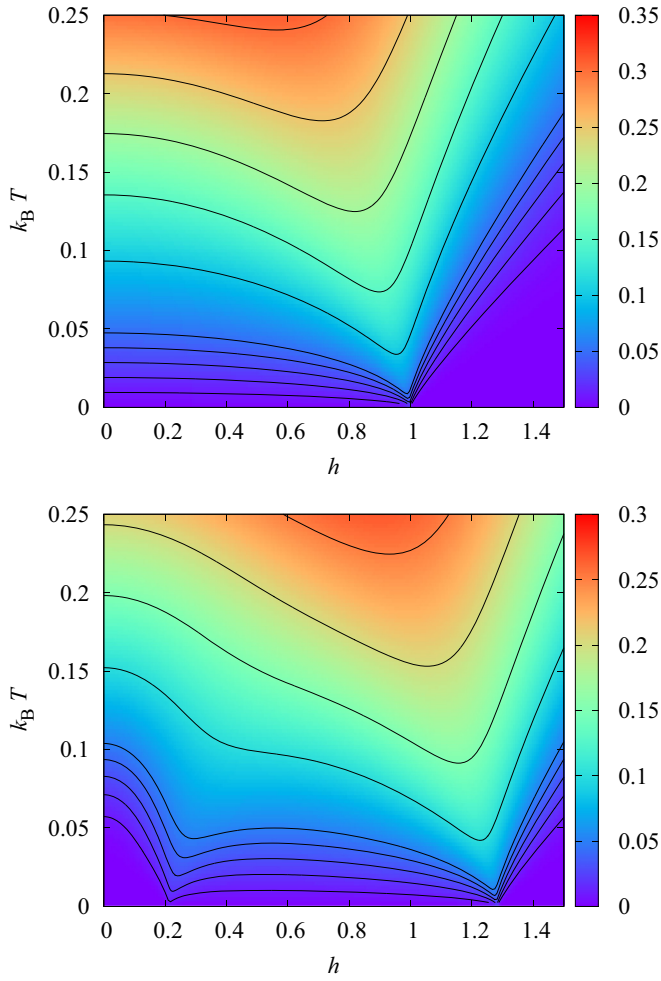

FIG. 14. Density plot of the entropy as a function of the magnetic field and temperature for the zigzag chain with $\theta = \pi/8$, $\varphi_E = \pi/16$, and $E = 0$ (top panel) and $E = 2$ (bottom panel). The curves with constant entropy correspond to $S/k_B = 0.01, 0.02, 0.03, 0.04, 0.05, 0.1, 0.15, 0.2, 0.25$.

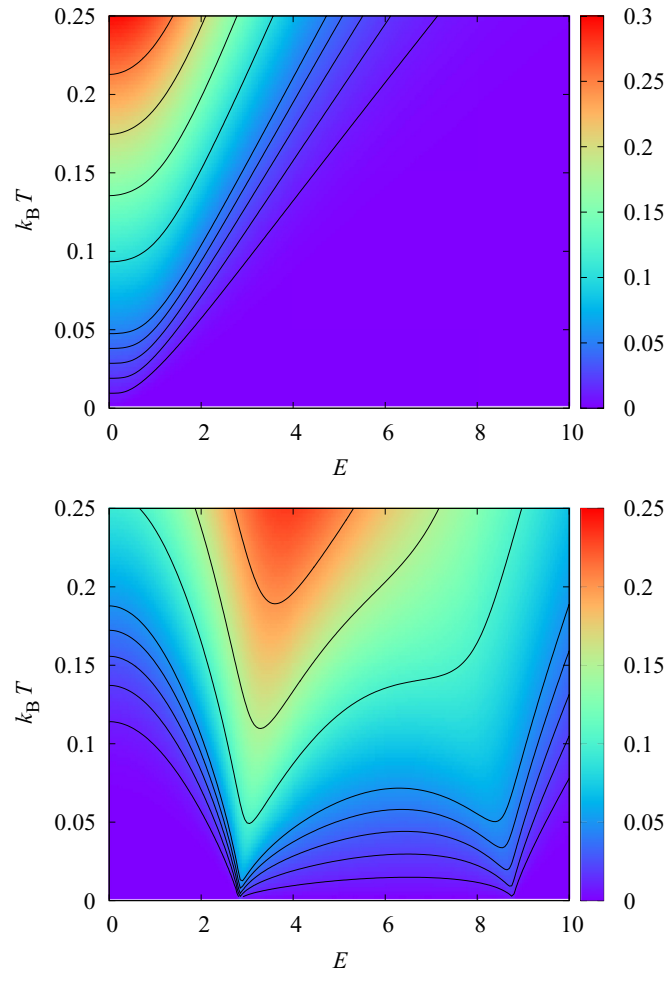

FIG. 15. Density plot of the entropy as a function of the electric field E and temperature for the zigzag chain with $\theta = \pi/8$, $\varphi_E = \pi/16$, and $h = 0$ (top panel) and $h = 1.5$ (bottom panel). The curves with constant entropy correspond to $S/k_B = 0.01, 0.02, 0.03, 0.04, 0.05, 0.1, 0.15, 0.2, 0.25$.

interesting case is the boundary of the spin-liquid phase ($h = J_\pm$), where the fermionic excitation spectrum touches zero, and therefore, low-energy excitations gain quadratic dispersion. It results in the square-root dependence of the specific heat $c \sim \sqrt{T}$.

The field-dependent specific heat is presented in Fig. 13. We see that low-temperature curves signal the quantum phase transitions by deep minima surrounded by two maxima in their vicinity.

The quantum spin paramagnets can also be attractive with respect to the enhanced magnetocaloric effect near critical fields [48–53]. Here the inclusion of the electric field provides an additional possibility to tune this effect and opens an opportunity to study the electrocaloric effect. The density plot for the entropy as a function of the magnetic field is shown in Fig. 14. For the case of the vanishing electric field, we get a simple XY chain, which is known to show an enhanced magnetocaloric effect near the saturation field (see, e.g., Ref. [48]). The application of the electric field in between the x and y axes opens the gap between two fermionic bands and leads to the additional field-driven quantum phase transition at low field. It is reflected by the steep slope of the isentropes at comparably small field. Therefore, the application of the electric field creates the possibility to govern the strength of the magnetoelectric effect in this case. The effect of the electric field on the entropy is also interesting to follow (see Fig. 15). We see that even for a small electric field the lines of constant entropy show a strong dependence on it. The application of the magnetic field changes the character of the dependence from heating to freezing.

VI. CONCLUSIONS

In the present paper we presented a rigorous consideration of the effect of the zigzag geometry on the properties of the quantum spin-$\frac{1}{2}$ XY magnetoelectric chain within the KNB mechanism. By virtue of the interplay of the geometry of the exchange interaction of the spins and the physics of the KNB mechanism the dielectric behavior of the system exhibits anisotropy. In addition to the usual off-diagonal components of the magnetoelectric tensor, α_{zx} and α_{zy}, the chain possesses

the diagonal, χ_{xx} and χ_{yy}, and off-diagonal, χ_{xy}, components of the electric susceptibility.

The ground-state phase diagram was studied. We revealed that the application of the electric field opens the gap in the excitation spectrum and leads to the appearance of the gapped zero-plateau phase. In general, the effect of the electric field is twofold: (i) it destroys the magnetic order, and (ii) it induces the gap in the spin-liquid phase.

We have also analyzed the direction of the polarization angle caused by the electric field and found that the applied magnetic field decreases (increases) it in the case when the angle of the electric field $\varphi_{\rm E}$ is smaller (larger) than θ. The behavior of the angle between the polarization vector and the direction of the chain (the x axis) can be nonmonotonous with respect to the magnitude and the direction of the applied electric field. When the direction of the external electric field is collinear with the chain bonds ($\varphi_{\rm E} = \theta$), the direction of the polarization is unaffected by the magnitudes of the electric and magnetic fields. Several cases of the universal dependence between the polarization and applied electric field angles were figured out in the limit of strong electric field.

In addition to the zero-temperature properties, we analyzed some thermal effects, particularly the temperature behavior of the specific heat for various regimes and its low-temperature electric and magnetic field dependence. The isentropes in both the (E, T) and (h, T) planes were presented. The features of the magnetocaloric and electrocaloric effects were discussed. We found that the appearance of the quantum phase transition at a low magnetic field with the application of the electric field is favorable for the enhanced magnetoelectric effect.

ACKNOWLEDGMENTS

The authors express their gratitude to O. Derzhko and T. Krokhmalskii for the valuable discussions. The present research was partially supported by the ICTP (OEA, network NT-04). O.B. and T.V. acknowledge the kind hospitality of the Yerevan State University in 2016. V.O. also acknowledges the partial financial support from the grants of the State Committee of Science of Armenia, Grants No. 13-1F343 and No. SFU-02. He also would like to thank the ICMP for warm hospitality during his visits to L'viv in 2016 and 2017.

APPENDIX A: POLARIZATION ANGLE FOR $\varphi_{\rm E} = \theta$

Let us consider a more general case of the XXZ magnetoelectrics on a zigzag chain defined by the Hamiltonian

$$\begin{aligned}\mathcal{H} &= \mathcal{H}_{xxz} + \mathcal{H}_E,\\ \mathcal{H}_{xxz} &= \sum_{j=1}^{N}\left[J_{xy}\left(s_j^x s_{j+1}^x + s_j^y s_{j+1}^y\right) + J_z s_j^z s_{j+1}^z - h s_j^z\right],\\ \mathcal{H}_E &= \sum_{j=1}^{N}[E_y\cos\theta + (-1)^j E_x \sin\theta] D_{j,j+1}. \end{aligned} \tag{A1}$$

For the sake of simplicity we introduced here the notation $D_{j,j+1} = (s_j^x s_{j+1}^y - s_j^y s_{j+1}^x)$.

In the case $\varphi_{\rm E} = \theta$, the electric field acts on the bonds which are noncollinear with the electric field:

$$\mathcal{H}_E = \sum_{j=1}^{N/2} E\sin(2\varphi_{\rm E}) D_{2j,2j+1}. \tag{A2}$$

Now, we use the standard notation for the thermal average:

$$\langle D_{j,j+1}\rangle = \frac{\mathrm{Tr}\{D_{j,j+1}\exp[-\beta\mathcal{H}(E\sin(2\varphi_{\rm E}))]\}}{\mathrm{Tr}\exp[-\beta\mathcal{H}(E\sin(2\varphi_{\rm E}))]}. \tag{A3}$$

We can introduce the spatial inversion operator I, which sets the opposite ordering of sites. Using the relations $I D_{j,j+1} I = -D_{j,j+1}$, $I\mathcal{H}_E I = -\mathcal{H}_E$, and $I\mathcal{H}_{xxz} I = \mathcal{H}_{xxz}$, one can show that

$$\langle D_{j,j+1}\rangle = -\frac{\mathrm{Tr}\{D_{j,j+1}\exp[-\beta\mathcal{H}(-E\sin(2\varphi_{\rm E}))]\}}{\mathrm{Tr}\exp[-\beta\mathcal{H}(-E\sin(2\varphi_{\rm E}))]}. \tag{A4}$$

To invert the sign before the electric field, we apply the transformation (3.2) with the following parameters:

$$\begin{aligned}\phi_{2j-1} &= \phi_{2j} = 2j\phi_0,\\ \tan\phi_0 &= E\sin(2\varphi_{\rm E}),\end{aligned} \tag{A5}$$

thus proving $\langle D_{2j-1,2j}\rangle = 0$. On the contrary $\langle D_{2j,2j+1}\rangle \neq 0$, and the polarization components $p_x = \sin\theta\langle D_{2j,2j+1}\rangle$ and $p_y = -\cos\theta\langle D_{2j,2j+1}\rangle$ direct the polarization perpendicular to the noncolinear bonds [see Eq. (4.10)].

It should be noted that the given arguments are not valid for the quantum spin chain with the next-nearest-neighbor interaction since the rotation (A5) affects the latter coupling.

APPENDIX B: POLARIZATION ANGLE FOR SMALL FIELDS

We consider again the Hamiltonian (A1) $\mathcal{H}(E_x\sin\theta, E_y\cos\theta)$. To get the polarization angle, we can expand the polarizations in small fields:

$$\begin{aligned}p_\mu &= \chi_{\mu x}E_x + \chi_{\mu y}E_y,\\ \chi_{\mu\nu} &= \frac{1}{N}\sum_{i,j}\left(\left\langle P^\mu_{i,i+1}P^\nu_{j,j+1}\right\rangle - \left\langle P^\mu_{i,i+1}\right\rangle\left\langle P^\nu_{j,j+1}\right\rangle\right);\end{aligned}$$

thus,

$$\tan\varphi_{\rm P} = \frac{\chi_{yx}\cos\varphi_{\rm E} + \chi_{yy}\sin\varphi_{\rm E}}{\chi_{xx}\cos\varphi_{\rm E} + \chi_{xy}\sin\varphi_{\rm E}}. \tag{B1}$$

Let us introduce the reduced quantities $\tilde{E}_x = E_x\sin\theta$, $\tilde{E}_y = E_y\cos\theta$, $\tilde{P}^x_{i,i+1} = P^x_{i,i+1}/\sin\theta$, $\tilde{P}^y_{i,i+1} = P^y_{i,i+1}/\cos\theta$, and

$$\tilde{\chi}_{\mu\nu} = \frac{1}{N}\sum_{i,j}\left(\left\langle\tilde{P}^\mu_{i,i+1}\tilde{P}^\nu_{j,j+1}\right\rangle - \left\langle\tilde{P}^\mu_{i,i+1}\right\rangle\left\langle\tilde{P}^\nu_{j,j+1}\right\rangle\right).$$

It is easy to see that $\chi_{xx} = \sin^2\theta\,\tilde{\chi}_{xx}$, $\chi_{yy} = \cos^2\theta\,\tilde{\chi}_{yy}$, $\chi_{xy} = \sin\theta\cos\theta\,\tilde{\chi}_{xy}$, $\chi_{yx} = \sin\theta\cos\theta\,\tilde{\chi}_{yx}$.

Next, we are going to prove that $\tilde{\chi}_{xy} = \tilde{\chi}_{yx} = 0$. The Hamiltonian and $\sum_i \tilde{P}^y_{i,i+1}$ are invariant with respect to the translation, while $\sum_i \tilde{P}^x_{i,i+1}$ changes sign after the one-site translation. It makes the correlation function $\sum_{i,j}\langle\tilde{P}^x_{i,i+1}\tilde{P}^y_{j,j+1}\rangle$ and the corresponding susceptibility $\tilde{\chi}_{xy}$ to zero. Finally, it is easy to prove that $\tilde{\chi}_{xx} = \tilde{\chi}_{yy}$. It follows from $f(E_x\sin\theta, E_y\cos\theta) = f(E_y\cos\theta, E_x\sin\theta)$, shown in Sec. III. Inserting it into Eq. (B1), we recover Eq. (4.13).

[1] Sh. Dong, J.-M. Liu, S.-W. Cheong, and Zh. Ren, Adv. Phys. **64**, 519 (2015).
[2] M. Fiebig, J. Phys. D **38**, R123 (2005).
[3] Y. Tokura, S. Seki, and N. Nagaosa, Rep. Prog. Phys. **77**, 076501 (2014).
[4] S.-W. Cheong and M. Mostovoy, Nat. Mater. **6**, 13 (2007).
[5] Y. Tokura and S. Seki, Adv. Mater. **22**, 1554 (2010).
[6] Y. Wand, J. Li, and D. Viehland, Mater. Today **17**, 269 (2014).
[7] N. Ortega, A. Kumar, J. F. Scott, and R. S. Katiyar, J. Phys.: Condens. Matter **27**, 504002 (2015).
[8] F. Matsukura, Y. Tokura, and H. Ohno, Nat. Nanotechnol. **10**, 209 (2015).
[9] Q. N. Meier, M. Fechner, T. Nozaki, M. Sahashi, Z. Salman, T. Prokscha, A. Suter, P. Schoenherr, M. Lilienblum, P. Borisov, I. E. Dzyaloshinskii, M. Fiebig, H. Luetkens, and N. A. Spaldin, arXiv:1804.07694.
[10] H. Katsura, N. Nagaosa, and A. V. Balatsky, Phys. Rev. Lett. **95**, 057205 (2005).
[11] C. Jia, S. Onoda, N. Nagaosa, and J. H. Han, Phys. Rev. B **74**, 224444 (2006).
[12] M. Brockmann, A. Klümper, and V. Ohanyan, Phys. Rev. B **87**, 054407 (2013).
[13] O. Menchyshyn, V. Ohanyan, T. Verkholyak, T. Krokhmalskii, and O. Derzhko, Phys. Rev. B **92**, 184427 (2015).
[14] J. Sznajd, Phys. Rev. B **97**, 214410 (2018).
[15] W.-L. You, G.-H. Liu, P. Horsch, and A. M. Oleś, Phys. Rev. B **90**, 094413 (2014).
[16] P. Thakur and P. Durganandini, in *Solid State Physics: Proceedings of the 59th DAE Solid State Physics Symposium 2014*, AIP Conf. Proc. No. 1665 (AIP, New York, 2015), p. 130051; in *DAE Solid State Physics Symposium 2015*, AIP Conf. Proc. No. 1731 (AIP, New York, 2016), p. 130051.
[17] P. Thakur and P. Durganandini, Phys. Rev. B **97**, 064413 (2018).
[18] Q.-Q. Wu, W.-H. Ni, and W.-L. You, J. Phys.: Condens. Matter **29**, 225804 (2017).
[19] S. Park, Y. J. Choi, C. L. Zhang, and S.-W. Cheong, Phys. Rev. Lett. **98**, 057601 (2007).
[20] S. Seki, Y. Yamasaki, M. Soda, M. Matsuura, K. Hirota, and Y. Tokura, Phys. Rev. Lett. **100**, 127201 (2008).
[21] A. A. Bush, V. N. Glazkov, M. Hagiwara, T. Kashiwagi, S. Kimura, K. Omura, L. A. Prozorova, L. E. Svistov, A. M. Vasiliev, and A. Zheludev, Phys. Rev. B **85**, 054421 (2012).
[22] Y. Qi and A. Du, Phys. Lett. A **378**, 1417 (2014).
[23] Y. Naito, K. Sato, Y. Yasui, Y. Kobayashi, and M. Sato, J. Phys. Soc. Jpn. **76**, 023708 (2007).
[24] Y. Yasui, Y. Naito, K. Sato, T. Moyoshi, M. Sato, and K. Kakurai, J. Phys. Soc. Jpn. **77**, 023712 (2008).
[25] F. Schrettle, S. Krohns, P. Lunkenheimer, J. Hemberger, N. Büttgen, H.-A. Krug von Nidda, A. V. Prokofiev, and A. Loidl, Phys. Rev. B **77**, 144101 (2008).
[26] S. Seki, T. Kurumaji, S. Ishiwata, H. Matsui, H. Murakawa, Y. Tokunaga, Y. Kaneko, T. Hasegawa, and Y. Tokura, Phys. Rev. B **82**, 064424 (2010).
[27] C. Lee, J. Liu, M.-H. Whangbo, H.-J. Koo, R. K. Kremer, and A. Simon, Phys. Rev. B **86**, 060407(R) (2012).
[28] S. Lebernegg, M. Schmitt, A. A. Tsirlin, O. Janson, and H. Rosner, Phys. Rev. B **87**, 155111 (2013).
[29] M. Azimi, L. Chotorlishvili, S. K. Mishra, S. Greschner, T. Vekua, and J. Berakdar, Phys. Rev. B **89**, 024424 (2014).
[30] M. Azimi, L. Chotorlishvili, S. K. Mishra, T. Vekua, W. Hübner, and J. Berakdar, New J. Phys. **16**, 063018 (2014).
[31] M. Azimi, M. Sekania, S. K. Mishra, L. Chotorlishvili, Z. Toklikishvili, and J. Berakdar, Phys. Rev. B **94**, 064423 (2016).
[32] S. Stagraczyński, L. Chotorlishvili, M. Schüler, M. Mierzejewski, and J. Berakdar, Phys. Rev. B **96**, 054440 (2017).
[33] F. Heidrich-Meisner, A. Honecker, and T. Vekua, Phys. Rev. B **74**, 020403(R) (2006).
[34] T. Vekua, A. Honecker, H.-J. Mikeska, and F. Heidrich-Meisner, Phys. Rev. B **76**, 174420 (2007).
[35] Sh. Furukawa, M. Sato, and Sh. Onoda, Phys. Rev. Lett. **105**, 257205 (2010).
[36] M. Sato, Sh. Furukawa, Sh. Onoda, and A. Furusaki, Mod. Phys. Lett. B **25**, 901 (2011)
[37] M. Sato, T. Hikihara, and T. Momoi, Phys. Rev. B **83**, 064405 (2011).
[38] A. K. Kolezhuk, F. Heidrich-Meisner, S. Greschner, and T. Vekua, Phys. Rev. B **85**, 064420 (2012).
[39] A. A. Zvyagin, Zh. Eksp. Teor. Fiz. **98**, 1396 (1990) [Sov. Phys. JETP **71**, 779 (1990)].
[40] M. Oshikawa and I. Affleck, Phys. Rev. Lett. **79**, 2883 (1997); I. Affleck and M. Oshikawa, Phys. Rev. B **60**, 1038 (1999).
[41] M. Bocquet, F. H. L. Essler, A. M. Tsvelik, and A. O. Gogolin, Phys. Rev. B **64**, 094425 (2001).
[42] J. H. H. Perk and H. W. Capel, Phys. Lett. A **58**, 115 (1976).
[43] O. Derzhko, J. Richter, and O. Zaburannyi, J. Phys.: Condens. Matter **12**, 8661 (2000).
[44] O. Derzhko and T. Verkholyak, J. Phys. Soc. Jpn. **75**, 104711 (2006).
[45] J. H. Taylor and G. Müller, Phys. A (Amsterdam, Neth.) **130**, 1 (1985).
[46] E. Lieb, T. Schultz, and D. Mattis, Ann. Phys. (NY) **16**, 407 (1961).
[47] J. Knolle and R. Moessner, arXiv:1804.02037.
[48] M. E. Zhitomirsky and A. Honecker, J. Stat. Mech.: Theor. Exp. (2004) P07012.
[49] C. Trippe, A. Honecker, A. Klümper, and V. Ohanyan, Phys. Rev. B **81**, 054402 (2010).
[50] M. Topilko, T. Krokhmalskii, O. Derzhko, and V. Ohanyan, Eur. Phys. J. B **85**, 278 (2012).
[51] B. Wolf, A. Honecker, W. Hofstetter, U. Tutsch, and M. Lang, Int. J. Mod. Phys. B **28**, 1430017 (2014).
[52] B. Wolf, Y. Tsui, D. Jaiswal-Nagar, U. Tutsch, A. Honecker, K. Remović-Langer, G. Hofmann, A. Prokofiev, W. Assmus, G. Donath, and M. Lang, Proc. Natl. Acad. Sci. USA **108**, 6862 (2011).
[53] M. Lang, B. Wolf, A. Honecker, L. Balents, U. Tutsch, P. T. Cong, G. Hofmann, N. Krüger, F. Ritter, W. Assmus, and A. Prokofiev, Phys. Status Solidi B **250**, 457 (2013).